Left Ventricular Strain from Myocardial Perfusion PET Imaging: Method Development and Comparison to 2-Dimensional Echocardiography

Jingwen Huang[1], Adam J. Mitchell[2], Ernest V. Garcia[3], C. David Cooke[3], Russell Folks[3], Maria Pernetz[4], Abhinav Goyal[2], Marina Piccinelli[3], and Jonathon A. Nye[3]

[1]Department of Medicine, Emory University School of Medicine, Atlanta, Georgia; [2]Department of Medicine, Division of Cardiology, Emory University School of Medicine, Atlanta, Georgia; [3]Department of Radiology and Imaging Sciences, Emory University School of Medicine, Atlanta, Georgia; and [4]Emory Adult Congenital Heart Center, Emory University School of Medicine, Atlanta, Georgia

This study aimed to develop a measure of longitudinal, radial, and circumferential myocardial strain at rest and regadenoson during pharmacologic stress using [82]Rb PET electrocardiography-gated myocardial perfusion imaging (MPI). **Methods:** We retrospectively identified 80 patients who underwent rest and regadenoson-stress CT attenuation–corrected [82]Rb PET and had a standard resting transthoracic echocardiogram (TTE) with global longitudinal strain (GLS) analysis within 3 mo. A method was developed to compute longitudinal, radial, and circumferential strain from PET MPI at stress and rest. PET MPI–derived strain and left ventricular function were compared with resting TTE measures as the clinical reference standard. Interobserver agreement of PET MPI strain and left ventricular ejection fraction processing was reported. **Results:** Longitudinal strain assessed with resting TTE GLS showed good correlation with PET MPI at stress ($r = 0.68$, $P < 0.001$) and rest ($r = 0.58$, $P < 0.001$). Resting TTE GLS also correlated with PET MPI radial strain at stress ($r = -0.70$, $P < 0.001$) and rest ($r = -0.59$, $P < 0.001$) and circumferential strain at stress ($r = 0.67$, $P < 0.001$) and rest ($r = 0.69$, $P < 0.001$). The left ventricular ejection fraction showed good correlation between resting TTE and PET MPI at stress ($r = 0.83$, $P < 0.001$) and rest ($r = 0.80$, $P < 0.001$). Bland–Altman analysis indicated positive bias of TTE GLS compared with PET MPI longitudinal strain at stress (mean difference = 5.1%, 95% CI = [−2.5, 12.7]) and rest (mean difference = 4.2%, 95% CI = [−4.3, 12.8]). Reproducibility of PET MPI longitudinal strain showed good agreement at stress (concordance correlation coefficient = 0.73, $P < 0.001$) and rest (concordance correlation coefficient = 0.74, $P < 0.001$), with Bland–Altman analysis showing a small bias in the longitudinal direction at stress (mean difference = −0.2%) and rest (mean difference = −1.0%). **Conclusion:** Strain measured with PET MPI using an automated technique correlated well with resting GLS strain obtained by TTE, and the measure is reproducible. Strain from PET MPI should be investigated further to establish reference ranges and assess its value in routine clinical practice.

Key Words: human; strain; PET; myocardial perfusion imaging; global longitudinal strain

Left ventricular ejection fraction (LVEF) is a proven measure of global left ventricular (LV) function that is associated with long-term outcomes. Cardiac diseases affect individuals differently and may not conform to arbitrary ejection fraction cutoffs. Therefore, the ability to further categorize a patient's LVEF is needed, particularly in a patient with an ejection fraction of 35%–50% (*1*). Regional LV function parameters such as wall motion and thickening have been shown to contribute incrementally to assessing LV function and categorizing patients' outcomes (*2*). Although powerful, these metrics do not provide 1 global parameter of LV function that can be easily understood and applied for measuring outcomes.

Echocardiography has an extensive track record in measuring myocardial deformation (i.e., strain). Strain analysis by echocardiography is a functional imaging tool for the clinical assessment of a range of cardiac pathologies. Global longitudinal strain (GLS) is most feasibly and robustly measured by speckle-tracking echocardiography and serves as a marker of global function that contributes incrementally to LVEF in the diagnosis and prognosis of cardiac disease (*3,4*). GLS has been shown by echo to be a superior predictor of all-cause cardiac mortality compared with LVEF in patients with coronary artery disease (*5*). In addition, GLS has been shown to be a robust measure for identifying early LV myocardial dysfunction, especially in patients undergoing chemotherapy (*6*).

Myocardial perfusion imaging (MPI), including PET and SPECT, is widely used in assessment of ischemic heart disease, determination of myocardial viability, and evaluation of cardiac device–related infections (*7*). Previously, we developed an automated approach to track the LV myocardium throughout the cardiac cycle to measure LV dyssynchrony using electrocardiogram (ECG) gated MPI (*8*). Here, we expand on this approach using this tracking methodology to measure radial, circumferential, and longitudinal strain at rest and during pharmacologic stress. We compare PET MPI strain measurements with resting GLS obtained by transthoracic echocardiography (TTE), considered to be the standard of care (*9,10*).

MATERIALS AND METHODS

Patient Population and Study Protocol

In this retrospective study, we investigated patients who underwent both TTE GLS analysis and rest and regadenoson-stress [82]Rb PET MPI within a 3-mo period at our institute between September 1, 2019, and September 1, 2021. Patients who had both studies were excluded if they had major cardiac events (e.g., myocardial infarction, cardiac surgery,

revascularization, valve intervention, or start of chemotherapy) between the time the 2 studies were completed. This study was approved by the Institutional Review Board of Emory University with a waiver of informed consent based on an assessment of no more than minimal risk.

Strain Measurements

2-Dimensional (2D) Echocardiography and Strain Analysis. Patients were imaged in the left lateral decubitus position with a commercially available echocardiography system (Vivid Seven E95; GE HealthCare). Image acquisition was performed using a 3.5-MHz transducer, at a depth of 16 cm in the parasternal view, and apical, 2-chamber, and 4-chamber views. Standard 2D, color Doppler, and M mode triggered to the QRS complex were saved in cine-loop format from 3 consecutive beats. The LV volumes (end systolic and end diastolic) were calculated from the conventional apical, 2-chamber, and 4-chamber views, and LVEF was calculated with the biplane Simpson rule (*11*). All measurements were made at rest by research personnel blinded to patient history and outcomes. Resting GLS measurement was performed on apical, 2-chamber, 4-chamber, and long-axis views using speckle-tracking echocardiography analysis on raw images obtained from patients in real time, and the images were analyzed with commercially available software (GE EchoPAC PC version 204), using 2D images at a frame rate between 55 and 65 fps. This software analyzed motion by tracking frame-to-frame movement of natural acoustic markers shown on standard ultrasonic images in 2D. Myocardial motion was analyzed using automated functional imaging software within EchoPAC to determine GLS. The LV endocardial border was traced at the end-systolic frame. The LV end-systolic frame was defined by the LV outflow tract Doppler at the closure of the aortic valve. If necessary, automatic endocardial detection was manually adjusted to assure correct tracking, excluding the papillary muscles and chordae and including the LV apex. Longitudinal strain curves were displayed, and experienced echo research personnel evaluated the image quality for satisfactory tracking of the borders.

[82]Rb PET MPI Study and Strain Analysis. ECG-gated [82]Rb PET MPI was performed on a Biograph 40 PET/CT (Siemens Medical Solutions) according to published guidelines (*12*). Patients were instructed to abstain from caffeine or xanthine-containing products for 12 h, as well as β-blockers and calcium channel blockers for 24 h. A low-dose CT scan was collected before the PET study for the purposes of attenuation correction. At rest, approximately 925 to 1,480 MBq of generator-produced [82]Rb-chloride, based on patient weight, was delivered intravenously via peripheral radial vein using an automated infusion system (Ruby-Fill; Jubilant Radiopharma). Hyperemia was induced by intravenous bolus infusion of regadenoson (0.4 mg/kg/min), followed by a second administration of [82]Rb-chloride at the time of peak heart rate. A total of 7 min of data were collected at rest and during hyperemia starting at the time of infusion. Static and ECG-gated images (8 temporal bins) were reconstructed with a non–time-of-flight 2D iterative order-subsets algorithm with attenuation and scatter correction using emission data starting at 2 min after infusion to the end of the data collection.

PET MPI strain measurements were performed using the short-axis LV endocardium detected and tracked throughout the cardiac cycle extracted from ECG-gated PET MPI studies (Fig. 1). Automatic detection of the LV endocardium was done using our standard 40 equiangular maximum count circumferential profile detection, followed by our count-based endocardial border modeling algorithm as used in the Emory Cardiac Toolbox (*8,10,13*). Strain measures were extracted on a point-by-point basis along the radial, circumferential, and longitudinal orientations on the rest and stress datasets.

Radial strain analysis uses the maximum count circumferential profiles extracted from short axis slices. The changes in these counts from each temporal frame along the cardiac cycle have been shown to be linear with myocardial thickening (*14*). The location of these samples is tracked as described earlier and then translated to the corresponding endocardial position depending on the measured thickening. The thickening for each sample in each frame is added to determine the radial strain at that temporal point. The average radial strain per frame is calculated as the sum of the strains per frame divided by the number of sample points. Global radial strain is then measured as the temporal maximum of this average strain.

Circumferential strain analysis uses the circumferential sample endocardial locations as in the radial strain described earlier. The spatial distance (L) between each pair of angular samples in each frame is calculated, and the samples' maximum separation over the cardiac cycle is assigned as L_o. For each pair of angular samples, strain is determined using the following standard equation: Strain $= 100\% \times (L - L_o)/L_o$ (*15*). The average strain is then determined on a segmental basis for each temporal frame in the cardiac cycle. The average of the sum of the
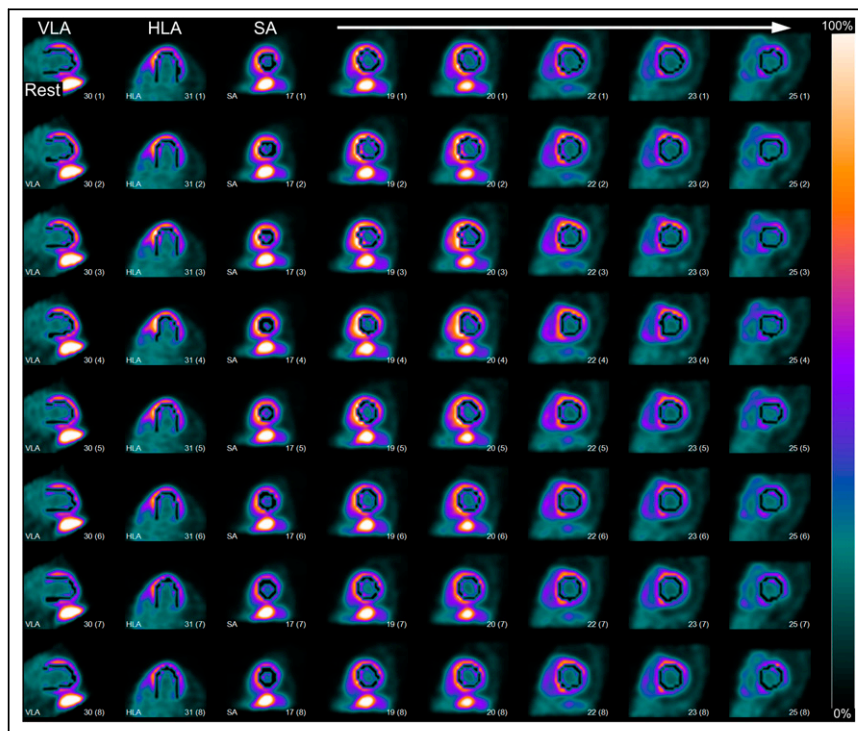

FIGURE 1. PET MPI strain autocontours. One patient example demonstrates PET MPI strain contouring methodology. Displayed images are LV endocardium detection and tracking overlay throughout cardiac cycle extracted from ECG-gated PET MPI under rest. Panels show representative vertical long axis (VLA) and horizontal long axis (HLA) slices, followed by short axis (SA) slices from apex to base along row (white arrow pointing left to right). End-diastolic frames are on top row, followed by contraction to end systole on middle rows and transitioning back to end diastole on bottom row. Color bar represents minimum to maximum normalized counts.

TABLE 1
Baseline Characteristics of Patient Population

Characteristic	Data
Age (y)	62 ± 12
Sex (men)	42 (52.5)
BSA (m²)	2.03 ± 0.3
Days between echocardiography and PET study	14.8 ± 31.7 (0–87)
Diabetes	30 (37.5)
Systolic BP (mm Hg)	132.0 ± 25.4
Diastolic BP (mm Hg)	76.1 ± 12.3
HFrEF	20 (25)
Ischemic cardiomyopathy	−16 (80)
Chemotherapy-induced cardiomyopathy	−2 (10)
Dilated cardiomyopathy	−1 (5)
History of heart transplant	−1 (5)
HFpEF	5 (6.3)
CKD	29 (36.3)
Prior MI	15 (18.8)

Data are number and percentage or mean ± SD.

BP = blood pressure; BSA = body surface area; CKD = chronic kidney disease; HFpEF = heart failure with preserved ejection fraction; HFrEF = heart failure with reduced ejection fraction; MI = myocardial infarction.

temporal minimum strain for the nonapical segments results in the global circumferential strain. Longitudinal strain analysis starts with the same endocardial samples used for the radial and circumferential strain calculations. These samples are then translated into 40 equiangular long axis planes. Each plane is defined by equidistant endocardial samples from apex to base. The distance between samples is given by the slice thickness, with the total number of samples given by the length of the LV. This length is different for each angle depending on the distance from base to apex and is different for each time frame as the LV contracts. This length is interpolated to 20 samples for each base-to-apex length of each of the 40 long axis planes and each of the 8 frames per cardiac cycle. The spatial distance (L) between each pair of interpolated longitudinal samples in each frame is calculated, and the samples' maximum separation over the cardiac cycle is assigned as L_o. The average strain per temporal frame is calculated by summing the strains over all samples over all longitudinal planes and dividing by the total number of samples. The GLS is then determined as the minimum strain over all temporal samples. Because both longitudinal and circumferential strains are negative numbers, their minimum yields the greatest magnitude of strain measured.

Circumferential and longitudinal strains were calculated in 2D within planes (e.g., within the short axis for circumferential strain) to correlate to 2D measurements by TTE. Radial thickening

as measured by the Emory Cardiac Toolbox is an inherently volumetric parameter, because it uses count changes throughout the cardiac cycle. These MPI volumetric radial strain measures were correlated to the 2D measures from TTE.

Interobserver Reproducibility

All PET MPI strain measures were computed twice by our research team (E.V.G. and R.F.), blinded to the patient condition to examine observer agreement. The Emory Cardiac Toolbox automatically determines processing parameters for the ungated study and uses these as the starting point for automatic selection of the gated parameters. Each observer had the option to adjust the apex and base slice selection and left ventricle center and radius for each of the 8 gated images. Selection of the base slice location was allowed to change by ±1 slice per gate. Stress and rest parameters, including total slices from base to apex, were matched as well as possible. Although all image parameters can affect quantitative results, in strain analysis, the most critical parameter appears to be base selection and how it is allowed to change during the cardiac cycle.

Statistical Analysis

Continuous variables are reported as mean ± SD or with 95% CI. Bland–Altman analysis, Pearson correlation, and the concordance correlation coefficient (CCC) were used to evaluate the association and agreement between resting TTE GLS and PET MPI longitudinal, radial, and circumferential strain and LVEF. CCC and Bland–Altman analysis were used to examine the interobserver agreement for all 3 PET MPI strain directions at stress and rest. In the interpretation of the CCC, a value below 0.4 is considered poor, a value between 0.4 to 0.7 is moderate, and a value greater than 0.7 is good agreement (16). For each CCC measure, the 95% CI is reported using the z-transform methods described by Lin (17). Evaluation of PET MPI strain differences at stress and rest for each direction were determined by examining for nonoverlapping Cis, which corresponds to a P value < 0.05.

RESULTS

Patient Population

A total of 85 patients were retrospectively identified, and 80 patients were included in our study. Three patients were excluded due to a major cardiac event (2 patients had ST-segment elevation myocardial infarction and 1 patient had coronary artery bypass surgery) between the PET MPI and the 2D TTE study. Two patients
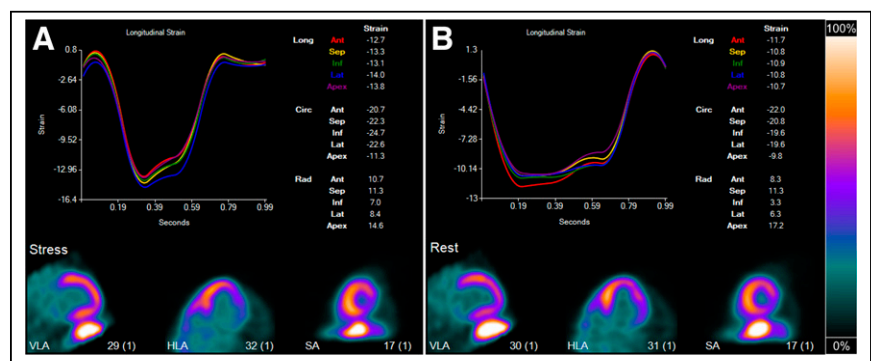

FIGURE 2. PET MPI strain. Longitudinal (Long) strain curves are from patient example in Figure 1 (stress [A] and rest [B]). Length of R-R interval has been normalized to 1 s. Strain plots over 1 cardiac cycle are color coded and reported for anterior (Ant), septal (Sep), inferior (Inf), lateral (Lat), and apical (Apex) regions. Circumferential (Circ) and Radial (Rad) strains are also displayed for corresponding myocardial walls but not plotted. Color bar represents minimum to maximum normalized counts. HLA = horizontal long axis; SA = short axis; VLA = vertical long axis.
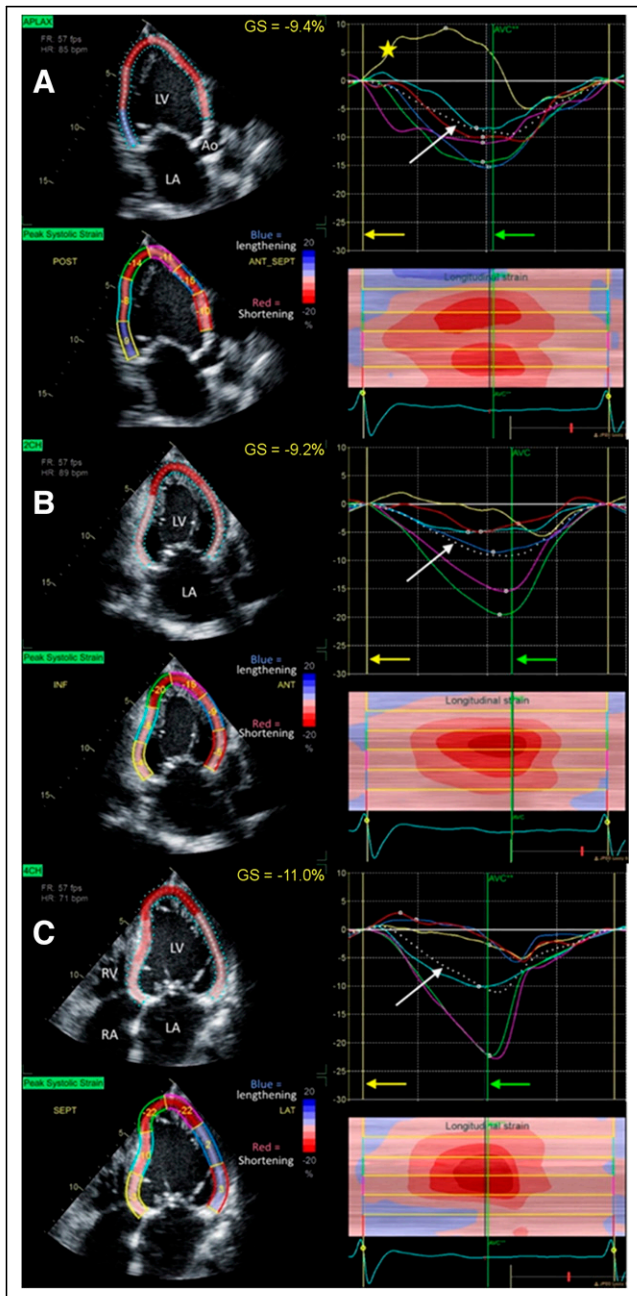
FIGURE 3. Resting TTE GLS. Rest 2D TTE strain measurements are from patient example in Figure 1. LVEF at rest was 32%, and GLS at rest was −9.9%. Three views—apical (A), 2-chamber (B), and 4-chamber (C)—are used in speckle-tracking echocardiography, and mean percentage longitudinal strain for each view is presented. Shades of red represent negative strain (contraction), whereas blue denotes positive strain (relaxation). White dotted line (white arrows) represents average strain among LV segments during cardiac cycle. Color of each trace line showing strain corresponds to anatomic color segments on 2D color image to left. Green arrows indicate aortic valve closure (AVC) line, which indicates end systole; yellow arrow shows end-diastolic (ED) line. Yellow star points out yellow curve on apical view; there is abnormal systolic lengthening of yellow segment (basal inferolateral segment). 2CH = 2-chamber; 4CH = 4-chamber; ANT = anterior; Ao = aorta; APLAX = apical long axis; FR = frame rate; GS = global strain; HR = heart rate; INF = inferior; LA = left atrium; LAT = lateral; POST = posterior; RA = right atrium; RV = right ventricle; SEPT = septal.

were excluded because PET MPI and 2D TTE were performed more than 3 mo apart. The final population ($n = 80$) consisted of 42 men and 38 women (mean age, 62 ± 12). The indications for PET MPI and TTE with strain analysis in these patients include chest pain (50%), preoperative evaluation or clearance (16%), dyspnea (14%), newly decreased ejection fraction (10%), abnormal ECG findings (4%), palpitations (3%), and syncope (3%). Patient characteristics and summary measures of 2D TTE and PET MPI are given in Table 1.

Strain Measurements

Figures 2 and 3 display the PET MPI strain and TTE processing at rest from a representative patient (80-y-old female with body mass index of 18.1 kg/m^2). In both techniques, strain curves are generated over the cardiac cycle, with the PET MPI including the longitudinal, radial, and circumferential directions. Table 2 summarizes the TTE GLS and PET MPI strain measurements. A greater degree of myocardial shortening is reflected by more negative longitudinal and circumferential strain values and more positive radial strain values.

Plots of resting TTE GLS compared with PET MPI strain at stress and rest in the longitudinal direction are shown in Figure 4, with the correlation and agreement summarized in Table 3. The associations of resting TTE GLS with PET MPI were good but showed low agreement, as indicated by the CCC. The low agreement can be explained by the presence of a bias between the 2 longitudinal strain measures, meaning that there is a difference in absolute scale

TABLE 2
Baseline Measures of LV Function from 2D TTE and PET MPI in Patient Population

| Parameter	Mean ± SD
2D TTE parameters	
Heart rate	75.8 ± 13.9
LVEF (%)	52 ± 14
LV GLS	−15.0 ± 4.7
End-diastolic LV diameter (cm)	4.8 ± 0.7
End-systolic LV diameter (cm)	3.5 ± 0.9
Interventricular septal thickness, diastolic (cm)	1.2 ± 0.3
LV posterior wall thickness (cm)	1.1 ± 0.3
LV mass index	107 ± 35
^{82}Rb PET ECG-gated MPI parameters	
Summed stress score	5.0 ± 7.2
Summed rest score	3.2 ± 4.9
Summed difference score	1.8 ± 4.2
Stress	
LVEF (%)	60.3 ± 16.1
Longitudinal strain	−19.7 ± 5.0
Radial strain	26.6 ± 10.2
Circumferential strain	−31.5 ± 12.0
Rest	
LVEF (%)	57 ± 15
Longitudinal strain	−18.8 ± 4.9
Radial strain	21.3 ± 8.0
Circumferential strain	−28.3 ± 10.3
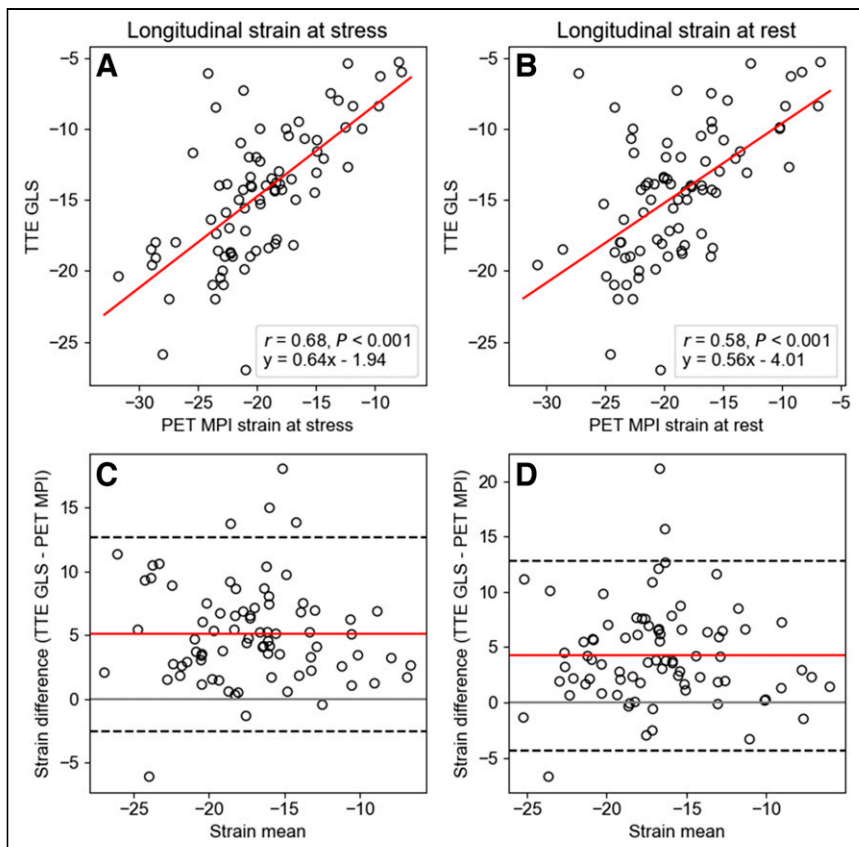
FIGURE 4. Longitudinal TTE GLS and PET MPI. (A and B) Linear regression plots showing correlation between longitudinal PET MPI and TTE GLS strain at stress (A) and rest (B), including equation of best fit. (C and D) Bland–Altman plots of longitudinal strain from resting TTE GLS and PET MPI at stress (C) (mean difference = 5.1%, 95% CI = [−2.5, 12.7]) and rest (D) (mean difference = 4.2%, 95% CI = [−4.3, 12.8]). Red line is mean measurement difference, and dashed lines are upper (mean +2 SD) and lower (mean −2 SD) limits of interval of agreement.

higher correlation of resting TTE GLS with PET MPI radial and circumferential strain at stress compared with rest, but this was not significant. The negative correlation with radial PET MPI strain is due to comparison of shortening in the longitudinal direction compared with lengthening in the radial direction. No other significant differences were observed between stress and rest PET MPI strain measures.

LVEF measured by resting TTE LVEF showed very good correlation with PET MPI at stress ($r = 0.83$, $P < 0.001$) and rest ($r = 0.80$, $P < 0.001$) and good agreement at stress (CCC $= 0.71$, $P < 0.001$) and rest (CCC $= 0.75$, $P < 0.001$) (Figs. 5A and 5B). Bland–Altman plots of LVEF from TTE GLS and PET MPI revealed a small bias at stress (mean difference $= −8.1\%$, 95% CI $= [−25.6, 9.4]$) and rest (mean difference $= −4.7\%$, 95% CI $= [−22.8, 13.5]$) (Figs. 5C and 5D).

Interobserver Reproducibility

Interobserver agreement of PET MPI strain processing from 2 experienced authors (E.V.G. and R.F.) was good for both stress (CCC $= 0.73$, 95% CI $= [0.56, 0.91]$) and rest (CCC $= 0.74$, 95% CI $= [0.55, 0.93]$). Bland–Altman plots show a minor bias between observers at stress (mean difference $= −0.2\%$, 95% CI $= [9.0, 8.5]$) and rest (mean difference $= −1.0\%$, 95% CI $= [−8.8, 6.8]$), indicating good reproducibility of the proposed method (Supplemental Fig. 2). Interobserver agreement of PET MPI strain processing in the radial and circumfer-

between the modality measures. This bias is more readily observed in Bland–Altman plots, as indicated by the nonzero mean of the measurement differences (Figs. 4A and 4B). We observed a bias in longitudinal strain between TTE GLS and PET MPI at stress (bias = 5.1%, 95% CI = [−2.5, 12.7]) and rest (bias = 4.2%, 95% CI = [−4.3, 12.8]) (Figs. 4C and 4D).

Plots of TTE GLS and PET MPI radial and circumferential strains are shown in Supplemental Figure 1, with the correlations summarized in Supplemental Table 1 (supplemental materials are available at http://jnm.snmjournals.org). There tended to be a

ential directions were higher than in the longitudinal direction, but differences were not significant (Supplemental Table 2).

DISCUSSION

In this study, we used PET MPI to compute LV strain in the longitudinal, radial, and circumferential directions at stress and rest. We then compared the strain measured by PET MPI to LV strain measured by 2D TTE. It was demonstrated that PET MPI–based strain measurements strongly correlate with strain obtained by echocardiography. A small bias was observed in the

TABLE 3
Correlation Coefficients between Resting TTE GLS and Strains Measured by PET MPI

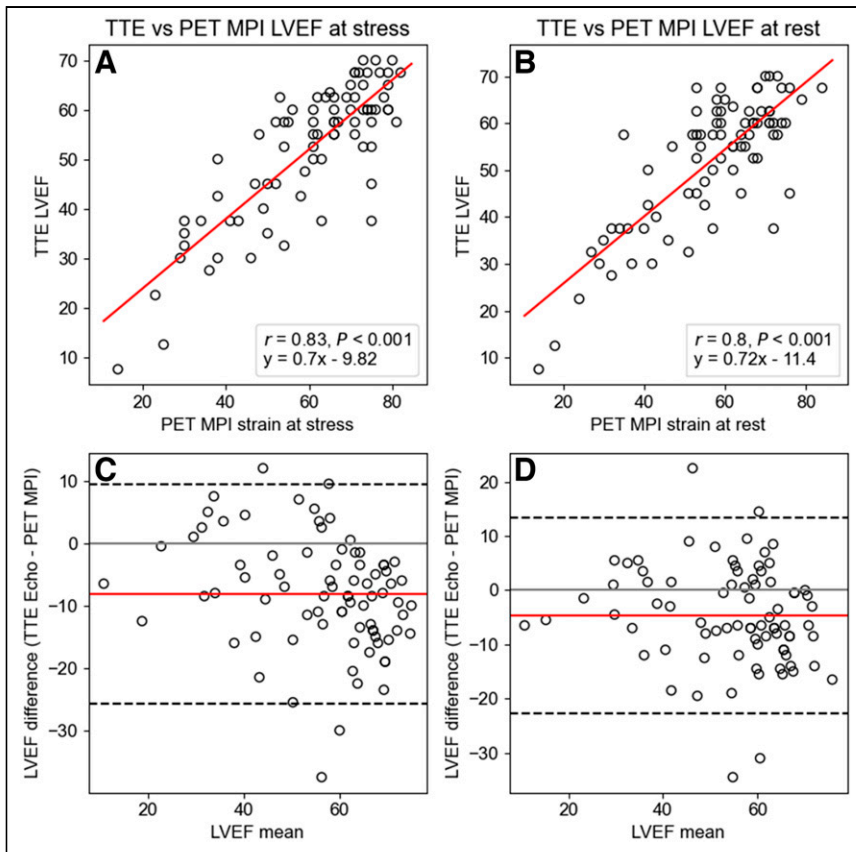|	Pearson coefficient	95% CI	P	CCC	95% CI	P
Stress						
Longitudinal strain	0.68	(0.54, 0.78)	<0.001	0.43	(0.30, 0.57)	<0.001
LVEF (%)	0.83	(0.73, 0.88)	<0.001	0.71	(0.52, 0.90)	<0.001
Rest						
Longitudinal strain	0.58	(0.41, 0.71)	<0.001	0.41	(0.27, 0.56)	<0.001
LVEF (%)	0.80	(0.70, 0.87)	<0.001	0.75	(0.55, 0.96)	<0.001

FIGURE 5. LVEF TTE and PET MPI. (A and B) Linear regression plots showing correlation between resting TTE and PET MPI LVEF at stress (A) and rest (B), including equation of best fit. (C and D) Bland–Altman plots of LVEF of resting TTE and PET MPI at stress (C) (mean difference = −8.1%, 95% CI = [−25.6, 9.4]) and rest (D) (mean difference = −4.7%, 95% CI = [−22.8, 13.5]). Red line is mean measurement difference, and dashed lines are upper (mean +2 SD) and lower (mean −2 SD) limits of interval of agreement.

longitudinal strain between the 2 modalities, indicating they were not identical on an absolute scale, but this was relatively small compared with the overall strain magnitude. Lastly, the interobserver reproducibility was lower in the longitudinal direction compared with the radial and circumferential directions, although these differences were not significant. Longitudinal strain is the most difficult of the 3 directions and is highly dependent on the operator's orientation of the valve plane, which can introduce additional error in the strain calculation, reducing the agreement. Other sources of error include differences in how the 2 datasets are measured, for example, 2D TTE vs. 3-dimensional (3D) MPI; operator preferences in positioning, particularly along the valve plane; and inherent error in the TTE GLS measure based on published test–retest data (*18*).

An important component of this study is the vendor and software package used to process strain from 2D TTE images. The algorithms used by the different echo manufacturers for measuring strain are considered intellectual property and have never been fully described. Ultrasound methods of measuring strain describe manual length measurements (*19,20*), tissue Doppler (*21*), speckle tracking (*22,23*), or a combination of techniques depending on the vendor package (*24*). This limitation may lead to significant variations among the results from the different manufacturers (*18*). Therefore, we have chosen to develop our PET MPI strain measures from basic principles. Differences in the calculation of strain

may partly explain the bias observed in the longitudinal strain comparisons, but the magnitude of this contribution is unknown. These challenges likely explain our observation of a bias between TTE GLS and PET MPI, which is not unique to our SPECT methods; a bias was also observed when compared with feature tracking with cardiac MRI (CMR) (*25*).

Speckle-tracking echocardiography has been shown as a useful tool and has been widely used in clinical studies in measuring heart functions, but some practical limitations to its use exist. First, for 2D strain echocardiography, because cardiac motion is a complicated 3D process involving rotation, contraction, and shortening, the direction of the movement occurs not only in the direction of the ultrasound beam but also in the direction of the cardiac muscle fiber orientation, creating potential bias. 3D speckle-tracking strain echocardiography has been developed, but challenges remain, such as lower frame rates and lower spatial resolution (*15,26*). Second, a recent study reported a head-to-head comparison of GLS measurements using speckle-tracking echocardiographic software packages from 7 ultrasound machine vendors and showed discrepancies in measuring strain among vendors (*27*). Third, radial and circumferential strain are not typically performed using echocardiography. Circumferential strain use has little incremental information, and radial strain is the least reliable and not recommended, with one of the reasons being that the amount of myocardium used for radial strain calculation is significantly less than that use longitudinal and circumferential directions (*15*).

In comparison to 2D TTE, PET MPI has the ability to measure global radial, circumferential, and longitudinal strain at both stress and rest and requires no extra information beyond what is collected by standard PET imaging. The use of PET imaging to measure LV strain has not been well established for routine clinical practice, but some publications demonstrated PET study–derived stain in potential clinical settings. Recent publications from Kawakubo et al. (*28,29*) showed the utility of ^{13}N-ammonia PET MPI to measure LV strain. They studied endocardial strain and used it to compare blood flow and myocardial motility in ischemic patients (*28*). This method was also used to evaluate right ventricular myocardial longitudinal strain to detect reduced right ventricular myocardial motion due to ischemia in the right coronary artery territory (*29*). Separately, Kawakubo et al. evaluated the LV strain in heart transplant patients and validated ^{13}N-ammonia PET strains using CMR feature tracking strains (*29*). Compared with previous studies, our study validates PET MPI–derived strain measurements with resting 2D TTE–derived strain. The addition of strain analysis to the usual PET MPI workflow could be clinically useful to detect subclinical heart failure, evaluate and monitor patients with cardiomyopathy, and further assist characterization of ischemic heart disease.

Several limitations need to be considered in this study. First, we only had 2D strain echocardiography to assess resting GLS and LVEF and correlate with PET strain data. Comparison with 3D echocardiographic strain would be preferred to overcome limitations with 2D TTE. PET study–derived strain can be further compared with CMR tagging using PET/MRI. CMR has been widely accepted as the reference standard imaging modality for strain quantification, with the advantage that deformation is directly measured by physical properties of the tissue (30). In addition, if the patient's blood pressure is significantly different between PET and TTE studies, this could contribute to differences of strain measurements. PET/CMR can overcome the blood pressure issue, because the imaging for both studies is processed simultaneously.

Second, there are technologic and physiologic differences in how strain studies were acquired, processed, and compared. TTE GLS and PET MPI measurements were obtained at 2 time points up to 3 mo apart. Only the resting GLS measurements by TTE were used as the reference standard to compare with stress and rest PET MPI measures of radial, circumferential, and longitudinal strain. Although it would be better to have compared all 3 strain directions individually, resting GLS was the only strain measurement available from the echocardiographic machine used in this study. Nevertheless, resting GLS is the main measurement established to add clinical information beyond LVEF. The rationale for comparing PET MPI measurements of longitudinal, radial, and circumferential strain to TTE measurements of GLS is the mechanical relationship between the 3 strains expressed mathematically as follows: (Global Radial Strain + 1) $\times$ (Global Circumferential Strain + 1) $\times$ (GLS + 1) = 1 (19). The rationale for comparing PET MPI measures of rest and stress to TTE measures at rest was to determine whether the increased counts in the stress MPI studies over the rest studies improved the correlations with TTE-derived strain and to determine changes in strain between rest and stress.

There are also technical differences between TTE and MPI in how strain is measured due to inherent differences in image formation. TTE has an advantage over MPI for defining the valve plane required for GLS measurements. GLS by TTE is determined from the average of myocardial wall measurements extracted from different planes acquired at different times during the scanning session, whereas MPI global strains are measured from simultaneous acquisition of all LV myocardial walls. MPI has an advantage over TTE in measuring radial strain since MPI uses a count-based method and does not rely on border detection. These technical differences can lead to differences in strain measurements.

Because ECG-gated PET MPI studies were acquired using 8 frames per cardiac cycle, these data are perceived to have low temporal resolution. Our tracking approach, which is common with our previous phase analysis tracking of the dyssynchrony of a specific LV segment, uses continuous Fourier functions to approximate the discrete wall thickening samples. This approach has been shown to have the equivalent temporal resolution of 64 frames per cardiac cycle (31). Nevertheless, although our measurement of myocardial strain is mostly count density dependent, the effect of increasing the number of frames per cardiac cycle to 16 or 32 while maintaining dose and acquisition time constant is yet to be determined. Another perceived limitation is that our count-based analysis cannot be performed in myocardial regions with extremely low tracer concentration due to infarction or severe stress-induced hypoperfusion. Our simulations have shown that our tracking approach can separate normal from abnormal thickening in regions with a count density as low as 5% of the average normal myocardial uptake

(10). Although the implication of these findings on the accuracy of strain measurements has yet to be established, the robustness of the tracking used to measure strain is well established.

CONCLUSION

We developed a methodology to measure radial, circumferential, and longitudinal strain from ECG-gated ^{82}Rb PET MPI studies. When compared with 2D TTE GLS, longitudinal PET MPI strain had good correlation and was reproducible between observers. There are currently no published reference normal strain values based on ^{82}Rb PET MPI studies, and this remains an area of needed development for clinical adoption.

DISCLOSURE

KEY POINTS

QUESTION: How does longitudinal, radial, and circumferential strain measured from ECG-gated ^{82}Rb MPI PET compare with resting 2D TTE GLS?

PERTINENT FINDINGS: Automatic detection of the LV endocardium for the extraction of strain from ECG-gated ^{82}Rb PET MPI is strongly associated with resting 2D TTE GLS. A greater degree of myocardial shortening is reflected by more negative longitudinal and circumferential strain values and more positive radial strain values, and the interobserver agreement of ECG-gated ^{82}Rb PET MPI strain at rest and stress was good.

IMPLICATIONS FOR PATIENT CARE: Longitudinal, radial, and circumferential strain can be reliably measured from ECG-gated ^{82}Rb MPI PET and may assist with the assessment of global LV function.

REFERENCES

1. Konstam MA, Abboud FM. Ejection fraction: misunderstood and overrated (changing the paradigm in categorizing heart failure). *Circulation.* 2017;135:717–719.
2. Cheitlin MD, Armstrong WF, Aurigemma GP, et al. ACC/AHA/ASE 2003 guideline update for the clinical application of echocardiography: summary article. A report of the American College of Cardiology/American Heart Association Task Force on Practice Guidelines (ACC/AHA/ASE Committee to update the 1997 guidelines for the clinical application of echocardiography). *J Am Soc Echocardiogr.* 2003;16:1091–1110.
3. Blessberger H, Binder T. Two dimensional speckle tracking echocardiography: clinical applications. *Heart.* 2010;96:2032–2040.
4. Zhang KW, French B, May Khan A, et al. Strain improves risk prediction beyond ejection fraction in chronic systolic heart failure. *J Am Heart Assoc.* 2014;3:e000550.
5. Antoni ML, Mollema SA, Delgado V, et al. Prognostic importance of strain and strain rate after acute myocardial infarction. *Eur Heart J.* 2010;31:1640–1647.
6. Sawaya H, Sebag IA, Plana JC, et al. Early detection and prediction of cardiotoxicity in chemotherapy-treated patients. *Am J Cardiol.* 2011;107:1375–1380.

7. Slart RHJA, Glaudemans AWJM, Gheysens O, et al. Procedural recommendations of cardiac PET/CT imaging: standardization in inflammatory-, infective-, infiltrative-, and innervation- (4Is) related cardiovascular diseases—a joint collaboration of the EACVI and the EANM. Summary. *Eur Heart J Cardiovasc Imaging.* 2020;21:1320–1330.

8. Chen J, Garcia EV, Folks RD, et al. Onset of left ventricular mechanical contraction as determined by phase analysis of ECG-gated myocardial perfusion SPECT imaging: development of a diagnostic tool for assessment of cardiac mechanical dyssynchrony. *J Nucl Cardiol.* 2005;12:687–695.

9. Santana CA, Folks RD, Garcia EV, et al. Quantitative ^{82}Rb PET/CT: development and validation of myocardial perfusion database. *J Nucl Med.* 2007;48: 1122–1128.

10. Cooke CD, Garcia EV, Cullom SJ, Faber TL, Pettigrew RI. Determining the accuracy of calculating systolic wall thickening using a fast Fourier transform approximation: a simulation study based on canine and patient data. *J Nucl Med.* 1994;35: 1185–1192.

11. Schiller NB, Acquatella H, Ports TA, et al. Left ventricular volume from paired biplane two-dimensional echocardiography. *Circulation.* 1979;60:547–555.

12. Dilsizian V, Bacharach SL, Beanlands RS, et al. ASNC imaging guidelines/SNMMI procedure standard for positron emission tomography (PET) nuclear cardiology procedures. *J Nucl Cardiol.* 2016;23:1187–1226.

13. Henneman MM, Chen J, Ypenburg C, et al. Phase analysis of gated myocardial perfusion single-photon emission computed tomography compared with tissue Doppler imaging for the assessment of left ventricular dyssynchrony. *J Am Coll Cardiol.* 2007;49:1708–1714.

14. Galt JR, Garcia EV, Robbins WL. Effects of myocardial wall thickness on SPECT quantification. *IEEE Trans Med Imaging.* 1990;9:144–150.

15. Marwick TH, Kosmala W. Strain imaging applications and techniques. In: Marwick TH, Abraham TP, eds. *ASE's Comprehensive Strain Imaging.* Philadelphia, PA: Elsevier; 2022:1–19.

16. Quinn C, Haber MJ, Pan Y. Use of the concordance correlation coefficient when examining agreement in dyadic research. *Nurs Res.* 2009;58:368–373.

17. Lin LI. A concordance correlation coefficient to evaluate reproducibility. *Biometrics.* 1989;45:255–268.

18. Mirea O, Pagourelias ED, Duchenne J, et al. Variability and reproducibility of segmental longitudinal strain measurement: a report from the EACVI-ASE Strain Standardization Task Force. *JACC Cardiovasc Imaging.* 2018;11:15–24.

19. Støylen A, Mølmen HE, Dalen H. Left ventricular global strains by linear measurements in three dimensions: interrelations and relations to age, gender and body size in the Hunt study. *Open Heart.* 2019;6:e001050.

20. Aurich M, Fuchs P, Muller-Hennessen M, et al. Unidimensional longitudinal strain: a simple approach for the assessment of longitudinal myocardial deformation by echocardiography. *J Am Soc Echocardiogr.* 2018;31:733–742.

21. Kuznetsova T, Herbots L, Richart T, et al. Left ventricular strain and strain rate in a general population. *Eur Heart J.* 2008;29:2014–2023.

22. Marwick TH, Leano RL, Brown J, et al. Myocardial strain measurement with 2-dimensional speckle-tracking echocardiography: definition of normal range. *JACC Cardiovasc Imaging.* 2009;2:80–84.

23. Sun JP, Lee AP, Wu C, et al. Quantification of left ventricular regional myocardial function using two-dimensional speckle tracking echocardiography in healthy volunteers: a multi-center study. *Int J Cardiol.* 2013;167:495–501.

24. Dalen H, Thorstensen A, Aase SA, et al. Segmental and global longitudinal strain and strain rate based on echocardiography of 1266 healthy individuals: the Hunt study in Norway. *Eur J Echocardiogr.* 2010;11:176–183.

25. Onishi T, Saha SK, Delgado-Montero A, et al. Global longitudinal strain and global circumferential strain by speckle-tracking echocardiography and feature-tracking cardiac magnetic resonance imaging: comparison with left ventricular ejection fraction. *J Am Soc Echocardiogr.* 2015;28:587–596.

26. Saito K, Okura H, Watanabe N, et al. Comprehensive evaluation of left ventricular strain using speckle tracking echocardiography in normal adults: comparison of three-dimensional and two-dimensional approaches. *J Am Soc Echocardiogr.* 2009; 22:1025–1030.

27. Farsalinos KE, Daraban AM, Unlu S, Thomas JD, Badano LP, Voigt JU. Head-to-head comparison of global longitudinal strain measurements among nine different vendors: the EACVI/ASE Inter-Vendor Comparison Study. *J Am Soc Echocardiogr.* 2015;28:1171–1181.

28. Kawakubo M, Nagao M, Yamamoto A, et al. ^{13}N-ammonia positron emission tomography-derived endocardial strain for the assessment of ischemia using feature-tracking in high-resolution cine imaging. *J Nucl Cardiol.* 2022;29: 2103–2114.

29. Kawakubo M, Nagao M, Kikuchi N, et al. ^{13}N-ammonia positron emission tomography-derived left-ventricular strain in patients after heart transplantation validated using cardiovascular magnetic resonance feature tracking as reference. *Ann Nucl Med.* 2022;36:70–81.

30. Garot J, Bluemke DA, Osman NF, et al. Fast determination of regional myocardial strain fields from tagged cardiac images using harmonic phase MRI. *Circulation.* 2000;101:981–988.

31. Chen J, Faber TL, Cooke CD, Garcia EV. Temporal resolution of multiharmonic phase analysis of ECG-gated myocardial perfusion SPECT studies. *J Nucl Cardiol.* 2008;15:383–391.